

DC-powered Fe^{3+} :sapphire Maser and its Sensitivity to Ultraviolet Light

Mark Oxborrow⁽¹⁾, Pierre-Yves Bourgeois⁽²⁾, Yann Kersalé⁽²⁾ and Vincent Giordano⁽²⁾

⁽¹⁾National Physical Laboratory
Hampton Road, Teddington, Middlesex TW11 0LW, United Kingdom
Email: mo@npl.co.uk

⁽²⁾Institut FEMTO-ST, UMR 6174 CNRS-Université de Franche-Comté
32 av. de l'Observatoire, 25044 Besançon Cedex, France
Email: vincent.giordano@femto-st.fr

INTRODUCTION

As realized early on [1] [2], the zero-field Fe^{3+} -doped-sapphire maser variant of the whispering-gallery-mode cryogenic sapphire oscillator (CSO) exhibits several alluring features: Its output is many orders of magnitude brighter than that of an active hydrogen maser and thus far less degraded by spontaneous-emission (Schawlow-Townes) and/or receiving-amplifier noise. Its oscillator loop is confined to a piece of mono-crystalline rock bolted into a metal can. Its quiet amplification combined with high resonator Q provide the ingredients for exceptionally low phase noise [3]. We here concentrate on novelties addressing the fundamental conundrums and technical challenges that impede progress:

(A) *Roasting*: The “mase-ability” of sapphire depends significantly on the chemical conditions under which it is grown and heat-treated. Beyond merely confirming previous work [4], we provide some fresh details and nuances.

(B) *Simplification*: This paper obviates the need for a Ka-band synthesizer: it describes how a 31.3 GHz loop oscillator, operating on the preferred WG pump mode, incorporating Pound locking, was built from low-cost components.

(C) *“Dark Matter”*: A Siegman-level [5] analysis of the experimental data determines the substitutional concentration of Fe^{3+} in HEMEX to be less than a part per billion prior to roasting and up to a few hundred ppb afterwards [4]. Chemical assays, using different techniques (incl. glow discharge mass spectra spectroscopy and neutron activation analysis) consistently indicate, however, that HEMEX contains iron at concentrations of a few parts per million. Drawing from several forgotten-about/under-appreciated papers, this substantial discrepancy is addressed.

(D) *Excitons*: Towards providing a new means of controlling the Fe^{3+} :saph. system, a cryogenic sapphire ring was illuminated, whilst masing, with UV light at wavelengths corresponding to known electronic and charge-transfer (thus valence-altering) transitions. Preliminary experiments are reported.

SAPPHIRE ROASTING TRIALS

In contrast to Czochralski growth, the 2050°C graphite heaters within a HEM growth furnace [6] produce a reducing atmosphere that induces oxygen vacancies and lowers the valence of ionic impurities. Roasting, *i.e.* annealing at high temperature in air, oxidizes Fe^{2+} ions inside this sapphire (back) to Fe^{3+} , though it is hypothesized here that the complete chemistry, as it affects ESR strengths, is more complicated than this process alone: the concentration and/or valencies of (i) defects (specifically F centers), (ii) individual impurities (*e.g.*, Ti, Mo), potentially connected to $\text{Fe}^{2+}/\text{Fe}^{3+}$ through charge-compensation, and (iii) $\text{Fe}^{3+}:\text{Fe}^{3+}$ clusters, amid a zoo of other combinations, will also be modified [7, 8].



Fig. 1: Lenton chamber furnace for sapphire annealing

Two HEMEX sapphire resonators, *viz.* Léonard and Basile (see Table 1), were received from FEMTO-ST. It was noticed that both contained optical striae. On mounting into a copper can of standard design, bolted directly to the second stage of a Cryomech PT405 pulse-tube cooler, both supported a WGH₁₇ doublet near 12.03 GHz, with Q s of around 60 million at 3 K, exhibiting slight bistabilities. On pumping on all candidate WG modes near 31.3 GHz with a Wiltron 6742B synthesizer boosted by an Agilent 83050A [2-50 GHz, 100mW] amplifier, neither sapphire ring could be gotten to mase. Both were subsequently subjected to roasting.

This was accomplished with a Lenton chamber furnace [9]; 200×200×200 mm sample space, maximum operating temperature 1700° C; MoSi₂ heating elements; programmable Eurotherm controller with Pt6Rh/Pt30Rh (type B) thermocouple. Each sapphire ring was cleaned (incl. soak in Piranha bath then DI rinse) and placed onto a 10-mm diameter alumina pedestal inside the chamber; a 100-mm diameter alumina beaker was thereupon placed over the ring to protect the latter from debris shedded by the furnace's liner and heaters. After roasting, Léonard contained a feint, internal milky “cloud” near its cylindrical surface, presumably oxidized impurities. Roasting did not noticeably alter the Q of either sapphire ring. Both mased on driving (down to 0 dBm) a variety of WG_{XX} pump modes near 31.3 GHz. Léonard exhibited bistable masing (dependent on coupling), the two modes of its WGH₁₇ doublet separated by 23 kHz.

Table 1	Ø [mm]	height [mm]	annealing schedule	(pump) WG _{XX} freq. [GHz]	signal (WGH ₁₇) freq. [GHz]	mode line- width [Hz]	maser output power
Léonard	50.017	30.018	16 hour @ 1600° C; 200° C/hr ramp up/down.	31.312570	12.0281059 12.0281082	199 241	-47 dBm -60 dBm
Basile	50.024	30.032	1 hour @ 1600° C (then broke) 200° C ramp up; passive cool.	31.340330	12.0267126	~200	-50 dBm

DC-POWERED Fe³⁺:sapph. MASER OSCILLATOR

Fig. 3 and Table 2 (+ Appendix) provide a detailed anatomy and “bill of materials”. The 31.3 GHz pump loop included many SMA-connectorized components (printed blue in Table 2), specified for operation over single frequency bands *below* 18 GHz. All components were screened against low-loss/spurions near 31.3 GHz prior to inclusion. The pump loop was powered by five Hittite MMIC amplifiers consuming 6.5 Watts (1.3 A at 5 V) in total.

Mode selector: This comprised a 6-pole (equi-ripple) 50-MHz bandwidth prefilter, (n) in Fig. 3 [retuned to 31.34 GHz; I.L. 3 dB] in series with a 3-pole, 17-MHz bandwidth filter (m) made from a 300-mm length of WR-28 waveguide; see Fig. 2. The latter was designed using [10], section 12.11; four inserted irises made from 0.2mm copper sheet, with ~2.5 mm (outer pair) and ~2.0 mm (inner pair) dia. holes, fixed with Epo-Tek H20E, formed its 3 $\lambda/2$: 35 $\lambda/2$: 3 $\lambda/2$ cavities.

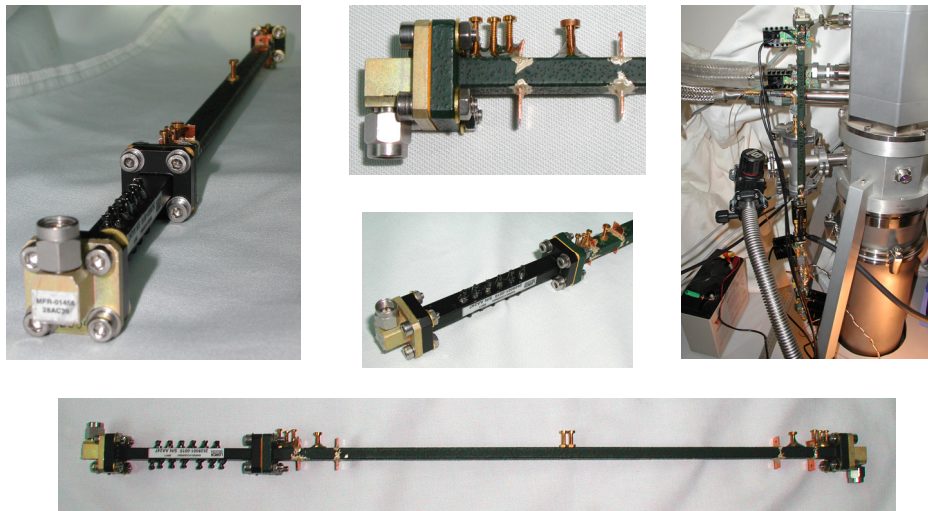


Fig. 2: WGxx mode-selection filter; top right image shows it mounted in situ.

Voltage-controlled phase shifter: On adjusting the manually-adjustable phase shifter (g), together with the bias voltages to each v.-c. attenuator (f), the carriers in each arm could be brought into balanced quadrature; the circuit provided 12° phase swing per volt [applied to its control circuit (y)], with ~0.3 dB/V residual a.m.; the I.L. was ~13 dB. The applied IF modulation @ 45.19 kHz gave symmetrical sidebands –15 dB down from the (recombined) carrier.

	Functional description	Make and model (+ supplier, if obscure)	Pertinent specifications and/or details (at relevant carrier frequency)
	Pump loop		$f_p \sim 31.3$ GHz
a/z	loop/stub probe	lab.-crafted from RG-405U semi-rigid	
b	cryo coax cable	RG178B/U, ~60cm in length	specified 1.4 dB loss per m @ 1 GHz, but ...
c	2-way power divider	ET Industries (Boonton NJ, USA) Model D-240-2; from SS	2-40 GHz; max I.L. 2.4 dB (specified); isolation 15 dB (2-way stripline); APC 3.5 connectors
d	wide-band driver amplifier	Hittite HMC635LC4 mounted on eval board;	specified 18.5 dB gain; power 1.4 W (280 mA @ 5 V); noise figure 6 dB
	voltage-controlled phase shifter:		overall insertion loss = -13.5 dB; phase swing from -1.0 V to +1.0 V = 24.56 degrees.
e	2-way power divider	narda Model 4316.2	12-18 GHz nominal; but measured IL @ f_p (excluding the 3dB of and ideal divider) ~1.5 dB
f	voltage-controlled attenuator	M/A COM Ltd; ML6550-N117-12; SPEC NO: 1085-06328; from SS	pair; one for each arm; 2-18 GHz; negative voltage operation; attenuation: 0 to -30 db
			"I" channel:
h	fixed phase shift	looped ~8 cm length of RG-402	
			"Q" channel
g	manually adjustable phase shifter	Spectrum C3117, LS-0212-1121; from SS	specification: 0-12 GHz operation; VSWR: 1.25 : 1 max; insertion loss: 0.4 db max; phase shift: 230° min; turns: 16
i	2-way power divider	narda, Model 4315.2	specified by manufacturer for 8.0-12.4 GHz operation only; but IL = -1.2 dB @ f_p measured.
j	manually adjustable phase shifter	MIDISCO MDC1089-1; http://www.microwavedistributors.com/ ;	0-18 GHz; phase adjustment span = $10^\circ \times \text{freq. (GHz)}$; $0.636^\circ \times \text{freq (GHz)}$ per revolution; max length = 2 1/2 inches; measured I.L. = 0.5 dB @ f_p
k	semi-rigid coax cable	standard RG 402 as above but ~20 cm long	
l	male SMA to WR-28 waveguide adapter	MDL (Microwave Development Laboratories) 190 ELECT; MFR-01456 28AC39; from TP	http://www.mdllab.com/ ; nearest-equivalent current MDL part: 28AC226.
n	retuned WR-28 waveguide BPF	LORCH (http://www.lorch.com/) 6WR28-31025/R50C; from TN	6-cavities (poles) in WR-28 straight, 79-mm long; originally centred on 31.025 GHz, 50 MHz bandwidth,
m	"mode-picker" WR-28 filter	modified 12" Flann Microwave WR28 waveguide section; from TP	see text for details; centre frequency 31.33522815 GHz; insertion loss 11.3 dB; -3 dB bandwidth 17.4 MHz.
o	medium power amp.	Hittite HMC499LC mounted on eval board;	13 dB gain @ f_p
p	3 dB hybrid	MA/COM FSC 96341, PN 2032-6374-00,	6.5–18.0 GHz; ISO port terminated by 50-Ω load
	Pound Servo		$f_{IF} = 45,189.5$ kHz; "base band" = 0-10 kHz
q	power detector	Agilent 8474E; negative response, 0.01-50 GHz response; 2.4-mm input connector;	± 0.4 dB up to 26.5 GHz; sensitivity > 0.4 mV/μW to 40 GHz
r	low pass filter	Mini-Circuits BLP 10.7	
s	ultra-low-noise rf amplifier	lab constructed, based Plessey SL561; powered by YUASA NP17-121 rechargeable 12 V battery	0.8 nV/√Hz input voltage noise; bandwidth 100 Hz to 6 MHz.; 40 dB gain
t	Balun	Mini-Circuits FTB1-1, BNC connectorized	0.2-500 MHz
u	double-balanced mixer	Hatfield Instruments (Plymouth England) Modulator Type 1754	freq. range: 0.01-100 MHz
v	IF frequency generator	Novotech (Seattle) Model DDS3	45.189.47 kHz; specified amplitude 0.7 Vpp into 50 ohms (or 0.88 dBm); 0 dBm measured.
w	servo loop filter = integrating amplifier	lab.-constructed; incorporating input-bias-voltage-nulled Burr-Brown OPA627.	input and output monitored with oscilloscope
x	passive LC bias-tee	lab.-constructed.	cross-over ~10 kHz
y	dual dc. bias + differential driver	lab.-constructed circuit; based around two OP177 op-amps	independently adjustable negative bias voltages.
	Maser signal chain		$f_M \sim 12.027$ GHz
α	armoured coax cable	Midwest Microwave CSY-SSSM-52-002 MA;	2m long
β	spectrum analyser	Anritsu MS2668C	9 kHz to 40 GHz coverage; clocked by 10-MHz maser ref.
γ	Isolator	Aerocomm (Bangkok, Thailand) J80.124	
δ	bandpass filter	Microphase R4815, bandpass filter, centre frequency = 12.0 GHz, BW = 140 MHz; from AX	specified -0.8145 dB @ 11.94 GHz; -0.9051 dB @ 12.08 GHz; measured -0.2dB @ 12 GHz; -65 dB @ 31.3 GHz
ε	low-noise amp	Herotek A1242-330	35 dB gain; noise figure: 3.0 dB; 12VDC, 350mA
ζ	3dB power splitter	Advance Technical Materials, Inc. (Patchogue, NY, USA) ATM 9216	8.0-12.4 GHz nominal
ω	spectrum analyzer	HP 8566B	2-22 GHz coverage
θ	Double-bal. mixer	Robinson Labs RL-7030-A-1	12-18 GHz nominal
τ	active hydrogen maser freq. reference	Sigma Tau MHM-2010; via two cascaded Spectral Dynamics, Inc. HPDA-15RM-C amplifiers	10 MHz output; along assorted lengths of Andrews Heliac, Times Microwave LMR-400 and RG213 cables around lab.
ρ	4-way passive splitter	Mini-Circuits FTB-1-1 balun into ZSC-4-1	~10 dBm from each ZSC-4-1 output port.
η	Synthesizer	Anritsu MG3692B signal generator	clocked by 10-MHz maser ref.
κ	rf amplifier	HP 461A	Mains powered; set to 40 dB gain
λ	frequency counter	Agilent 53132A	clocked by 10-MHz maser ref.

Table 2

Performance: On applying current to its amplifiers, the pump loop would reliably oscillate (and Pound-lock), provided the resonator's temperature lay below 20 K. On switching off the cooler, masing would persist up to 29.5 K. The Pound detector diode (q) lay outside of the cryostat. As inferred from a germanium resistance sensor attached to the resonator's can (read with a Lakeshore 340 temperature controller), the resonator's temperature "yoyoed" with an amplitude of ~ 0.1 K at the cooler's cycle frequency (~ 1.4 Hz); a corresponding yoyoing was observed on the Pound error signal. Even when Basile was stationed at its frequency turnover temperature (8.72 K; curvature of -11.85 Hz/K²) the affects of the cryocooler's thermal/mechanical vibrations still dominated; the measured Allan deviation at 10s was around 10^{-13} .

BROADENING MECHANISMS

Qualitatively, the observed weakness of the Fe³⁺:sapph.'s ESRs is due to spectral (as well as spatial) hole burning. The rational design of any device based on them requires that the hole burning's dependence on variables within experimental control be quantified. This boils down to determining the values of various time constants. Where data specific to Fe³⁺:sapph is lacking, estimates can be inferred from studies on (dilute) ruby; see Table 3.

Inhomogenous (or rather "heterogenous") broadening T_2^ :* In the limit of low doping concentrations, Fe³⁺:sapph. consistently exhibits total linewidths of a few tens of MHz, characterized by a time constant T_2^* of around 10 ns; crystal quality (Verneuil, Czochralski, HEM, ...) makes little difference. This intrinsic broadening is due to the hyperfine interaction between each Fe³⁺ ion and the (magnetic dipole's of the) ²⁷Al nuclei that surround it. Considering just the first 13 nearest nuclei, Wenzel predicted its magnitude of this broadening quite accurately [11]. Mössbauer spectroscopy (on ⁵⁷Fe³⁺-doped sapphire) [12] subsequently clarified the earlier ESR-measurements [13]. ENDOR experiments [14, 15] motivated the concept of a "frozen core" of nuclei surrounding each Fe³⁺/Cr³⁺ ion.

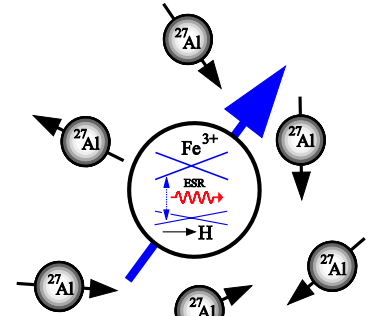


Fig. 4

Spin-lattice relaxation T_1 : This parameter is also well understood [16]; it does depend on crystal quality (see Table 3.)

Spin-spin (transverse) relaxation T_2 : One problem, on the experimental side, is that most of the (surprisingly limited) relevant experimental data comes from measurements on ruby at >10 ppm concentrations. A compounding problem, on the theoretical side, is that Cr³⁺:sapph at high (saturating) drive powers is known to violate Bloch theory -as based on the value of T_2 obtained from spin-echo ESR/ENDOR/PENDOR measurements. Even the exact shape of the homogenous broadening is still not wholly clear [17]. Acknowledging these caveats and persisting mysteries, we limit our sights to extracting a "ball-park" magnitude (for both the pump and signal transitions). The available literature indicates that, at least down to concentration levels of a few tens of ppm, the homogenous broadening of the Cr³⁺:sapph. ESRs, as quantified by T_2 , is still controlled by Cr:Cr electronic spin flip-flops. The value of T_2 has been measured through a variety of techniques –see Table 3. What is essential to understand here is that T_2 is not simply a constant but a function of (amongst other parameters) the concentration and the drive power, *i.e.*, intensity-broadening [18] has to be included. Though violations have been observed [19], to first, rough-and-ready approximation, the homogenous broadening scales proportionally to the square-root of the concentration: $T_2 \propto 1/\sqrt{\text{conc.}_{\text{Fe}^{3+}}}$. Within Bloch theory (BT), the spreading of an excitation due to intensity broadening is quantified by [18]:

$$\Delta f = \frac{\sqrt{1+S^2}}{\pi T_2}, \quad (1)$$

where $S = \chi \sqrt{T_1 T_2}$ is the degree of saturation, a.k.a. the dimensionless intensity; $\chi = (\gamma/2) \sqrt{\sigma \sigma^*} H$ is the Rabi frequency; γ is the "free spin" ESR field-to-frequency conversion factor (28 GHz per Tesla); $\sqrt{\sigma \sigma^*}$ is the (magnitude of the) dipole strength for the transition concerned; H is the magnetic field amplitude.

Beyond Bloch theory, the phenomenon of spin diffusion [20] needs to be included (as through the Yamanoi-Eberly model [21] or similar), but no attempt to chart these depths will be made here. Despite addressing optical hole burning, [22] reviews what is known about spin diffusion from ESR measurements. These works study Cr³⁺:sapph. in setups where the homogenous broadening grows less quickly with intensity than what BT predicts. The spin diffusion here is presumed to be driven by flip-flopping of the ²⁷Al nuclei spins, particularly those close-lying ones in the frozen core, whose flips can "jolt" the ESR of an individual Cr³⁺/Fe³⁺ ion far out of resonance from its pump/single WG mode. Using nuclear spin echo in conjunction with pulsed optical excitation of ruby's R1 line, the dephasing time(s) of the ²⁷Al : ²⁷Al

flip-flops have been measured [22, 23] for both the frozen core and bulk –see Table 3; it is worth noting here that both times are smaller than T_1 , suggesting that a pumped $\text{Fe}^{3+}:\text{sapph}$ ion will typically diffuse around the whole of the heterogenous linewidth before it non-radiatively decays. Needless to say, these measurements and insights are highly relevant to predicting the effective fraction of $\text{Fe}^{3+}:\text{sapph}$ ions that participate in maser action.

Property	Technique	Experimental particulars	Value	Ref.
inhomog. linewidth = $1 / \pi T_2^*$	X-band ESR spectroscopy	50 ppm Fe^{3+} 100-200 ppm Fe^{3+}	27 ± 5 MHz 28 MHz	[24] [25]
	Theoretical	for Cr^{3+} (magnetic field parallel to C axis)	10 Gauss = 28 MHz	
	Mossbauer spectroscopy	800 ppm $^{57}\text{Fe}^{3+}$	" 9.0 ± 3.0 Gauss" = 25 ± 8 MHz.	[12]
T_1	X-band ESR saturation-relaxation @ ~ 9 GHz	50 ppm Fe^{3+} conc.	7 ± 2 ms	[26]
	@ 9-10 GHz	200 ppm conc.	8 ± 1 ms	[25]
		20 ppm conc.	12 ± 1 ms	[25]
	@ 9.27 GHz	residual; Verneuil (vap.-phase)	20 ms	[27]
T_2	echo-ENDOR; @16 and 9.3 GHz	0.005-wt% ruby	1.5 μs	[28] [28]
	echo-PENDOR @ 693.4 nm (R_1 line)	0.005-wt% ruby	3.5 μs	[29] [28]
	free induction decay (FID) of ESR spin @ 5.9 GHz	0.009-wt % ruby	7.5 ± 7 μs	[21]
	optical hole burning of R_1 line @ 693.6 nm	0.0034-wt % ruby	15 μs	[22]
$\sqrt{(T_1 T_2)}$	microwave bistability		4.6 ± 0.2 μs	[30]
T_2 of ^{27}Al	nuclear spin-echo decay	in the "frozen core"	1 ms	[23]
		in the bulk	60 μs	ibid.
spin-spin (intraline cross-) relax. time	optical hole burning	0.05 wt% ruby	0.5 ms	[31]
Cr-Cr spin-flip time (reson. cross relax.)	many and various		1-50 μs	Table 1 in [23]
spectral diff. time T_d			14 μs	[22, 32]

Table 3: Key design parameter for $\text{Fe}^{3+}:\text{sapphire}$ maser action

A final insight comes from the observation of bi-mode masering: WG modes separated by 8 MHz coexist independently [4], whereas modes stationed 10 kHz apart compete (for the same population inversion) [33] as they brighten. This suggests that the effective homogenous linewidth lies below 10 kHz at low powers and somewhere between 10 kHz and 8 MHz at high powers.

Distilling Table 3 and the above insights into ball-park figures: Given the low concentration levels of Fe^{3+} ions in HEMEX, T_2 at low-power should be several tens of μs (say ~ 80 μs), corresponding to a homogenous linewidth of a few kHz (say ~ 4 kHz). With such a narrow homogenous linewidth, spin diffusion seems likely to be significant: the time, T_d , an $\text{Fe}^{3+}:\text{sapph}$ ion typically stays within the homogeneously broadened line risks being the same order of magnitude, if not shorter, than T_2 itself. At finite power, the key parameter is the Rabi frequency, χ , as given by (1) above, where the magnetic field amplitude can be estimated through $H \approx \sqrt{QP/(\mu_0 f_0 V_{\text{eff}})}$, where QP , f_0 and V_{eff} are the electromagnetic (co-circulating) power, frequency and effective volume of the WG mode in question. Compared to an X-band Ramsey cavity in a Cs clock, the extremely high Q s and smaller volumes of WG modes in cryogenic sapphire rings stand to elevate χ well above the tens-of-kHz Rabi frequencies encountered with the former. *Getting more quantitative (for the pump transition):* assuming an applied power of 1 mW, critical coupling, an effective mode volume of 5 cm^3 , a (loaded) Q of 1 billion; and noting that the transition amplitude of the (level-crossing thus somewhat forbidden) pump transition is only 0.05 in free spin units [26] [34], one arrives at an estimated Rabi frequency of around 1 THz; in comparison with any reasonable estimate of $1/\sqrt{(T_1 T_2)}$, this puts the saturation $S \gg 1$ corresponding to the whole inhomogeneously broadened line being made accessible; Fig 6.3 and its surrounds discussion in [18] clarify these remarks. The extent to which spin-diffusion will cripple the power broadening [21], remains to be quantified.

ULTRAVIOLET SENSITIVITY

The purpose of these experiments was to see whether either the number density or paramagnetic state of $\text{Fe}^{3+}:\text{sapph.}$ could be affected by light (at lowish intensities). Many workers with interests ranging from mineralogy to gravitational wave detection have measured optical absorption spectra of sapphire specimens [35] [36]. However, because optical transitions from $\text{Fe}^{3+}:\text{sapph.}$'s electronic ${}^6\text{S}$ ground state are doubly forbidden, they are often masked by stronger absorptions associated with other colour centres; Refs. [37] and [38] do nevertheless make explicit identifications. In particular, they observe a relatively strong and sharp " $4T_2^b$ " absorption line at 387 nm (at 77K). Although, to the best of the authors' understanding, $\text{Fe}^{3+}:\text{sapph.}$ is not expected (at zero applied magnetic field ...) to exhibit any sort of paramagnetic circular dichroism --as would facilitate state-selective optical pumping, the extreme ease with which radiation at this wavelength (or thereabouts) can be generated with an AlN light-emitting diode motivated the shining of some of it onto the sapphire ring --just to see what might happen. This was done using a room temperature diode feeding a plastic light pipe. See Figs. 2, 5 and Table 4. A diode of the same type was also mounted on the inner wall of the copper resonator can --see right image of Fig. 5 immediately below.

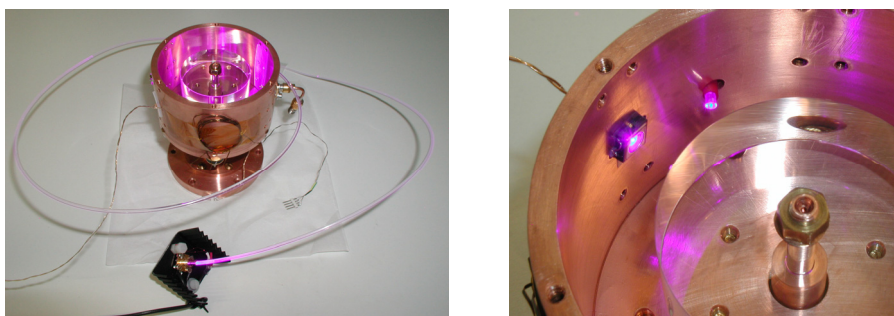


Fig.5: 385 nm optical excitation

As for the effects of even shorter-wavelength light, Tippins [39] studied the UV absorption spectrum of $\text{Fe}^{3+}:\text{sapph.}$ associated with valence-changing transitions: $\text{O}^- + \text{Fe}^{3+} \rightarrow \text{O}^- + \text{Fe}^{2+}$. In particular, he found a broad absorption around 255 nm associated with adding a spin-down electron to the so-called $t_{2g}(\pi^*)$ molecular anti-bonding orbital. Optically stimulating this chemical transition should reduce, temporarily, the density of Fe^{3+} ions thus the strength of their associated ESRs/masing. Again, as luck would have it, the required radiation can easily be gotten from the 254-nm line of a mercury vapour lamp. The only challenge comes in conveying it to the cryogenic sapphire ring efficiently. On removing the "lid" of the resonator can, this was done with a crystalline quartz window on the cryostat's AVC and two fused-silica convex lenses mounted within the cryostat; see Figs. 2 and 6 and Table 4.

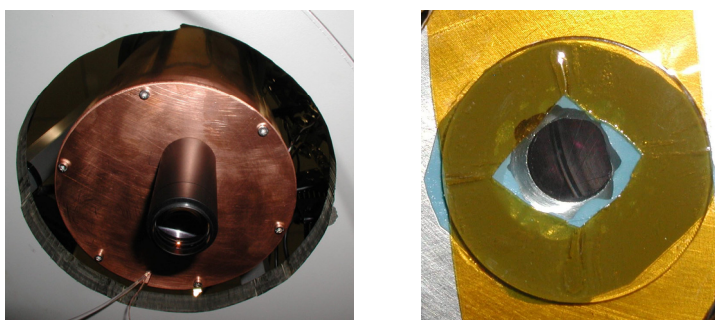


Fig 6: UV optical access of masing cryogenic sapphire ring; left: cryogenic lens assembly; right: image of cryogenic sapphire ring seen through this assembly (the circular lower and upper edges of the ring can both be seen).

Results. Alas, all negative! The 385 nm LED inside the copper can did not function (no light) when cold. The only noticeable effect upon injecting 385 nm radiation via the plastic light pipe was a slow transient shift in the maser frequency (taking several seconds to complete) consistent with heating. The optical power at 255 nm shone onto the sapphire crystal was estimated to be 1.63 mW (see Table 4 below). This could be turned on and off within a few tens of ms with a mechanical shutter. No substantial difference in the maser signal power could be detected when toggling between an open and closed shutter. The results of these optical-illumination experiments are, needless to say, preliminary. Using lasers or installing an optical build-up cavity would drive the excitation to $t_{2g}(\pi^*)$ harder; synchronous

detection would help to detect a weak effect. It is both salutary and intriguing to note that the ESR strengths of Cr^{3+} :sapph. (*i.e.* ruby) were not altered upon irradiating it with sufficient ^{60}Co γ rays to turn it orange in colour [40].

	Function	Make and model	Pertinent specifications and/or details
	385 nm stimulation:		
A	385nm UV diode	Nichia, NCSU034A	output centred on 385nm, width $\sim 10\text{nm}$; 3.8 V applied, 330 mA drawn.
B	Plastic light pipe	Mitsubishi “Eska” acrylic (PMMA) fibre, 2mm O.D.	1.2 m long; attenuation @385 nm (extrapolated from measurements $> 400\text{ nm}$): 700 dB/km; so attenuation through pipe used $\approx 0.84\text{ dB}$
	254 nm simulation:		
C	255 nm mercury vapour lamp	UVP Pen-Ray lamp, model 90-0012-01 (+ 11SC-1)	housed within $\sim 9\text{ mm}$ dia. aluminium shield with $0.19 \times 1.5''$ window.
D	Quartz window	lab. heirloom; orientation unknown; 1'' dia.; 2mm thick.	originally fine ground; hand polished against 1-micron “aloxite” held in damp cotton cloth, followed by 0.3 micron cerium oxide in same.
E	Fused silica lens	1'' diameter, plano-convex, focal length 50 mm nominal	manufacturer unknown; probably Spectrosil.
F	lens tube	Thorlabs SM1 series aluminium lens tubes of 1'' dia. optics	combination of SM1L05, + SM1L20 + SM1L30 stacked together; mounted through hole in first-stage rad-shield
G	Fused silica lens	1'' diameter, bi-convex, focal length 50 mm nominal	manufacturer unknown; probably Spectrosil.
	From http://uvp.com/mercury.html : typical intensity of Pen-Ray lamp (over the 254 nm line) at a distance of $0.75'' = 4.5\text{ mW/cm}^2$. However, “in the case of mercury lamps, the primary emissions peak at 254nm will decrease steadily with time due to quartz solarization. This will yield a net output of approximately 70% after 2,000 hours. The effect will then stabilize for the remainder of the life of the lamp.” So make that 3 mW/cm^2 . From measured experimental geometry, effective diameter of first silica lens (E) projected onto sphere $0.75''$ -radius sphere around from PenRay lamp $\approx 9.525\text{ mm}$. Transmission losses: $\sim 3.37\%$ reflection loss per surface from three pairs of surfaces plus absorption through $2\text{ mm} + 6\text{ mm} + 6\text{ mm}$ of silica @ -0.5% per mm (see http://www.uqgoptics.com/) ; compounding gives $\sim 24\%$ loss in total. Thus optical power projected into sapphire ring estimated to be: $\pi \times (0.9535/2)^2 \times 3 \times (1 - 24/100) = 1.63\text{ mW}$		

Table 4

Acknowledgements

MO wishes to thank several NPL colleagues: Conway Langham for enlarging the cryostat’s sample space; John Howes and David Gentle for loan of microwave equipment; and Roger Morrell for his assistance with the roasting.

Appendix

	Supplier
AX	Abex (UK) Ltd; www.abex.co.uk ; tel: +44 1252 844902; email: sales@abex.co.uk ; Abex (UK), Warren Close, Hartley Wintney, Hook, Hampshire, RG27 8DS, United Kingdom
SS	Solid State Electronics (UK); http://www.ssejim.co.uk/ ; tel: +44 2380 769598; e-mail: solidstate@ssejim.co.uk ; 6 The Orchard, Bassett Green Village, Southampton, SO16 3NA, United Kingdom
TP	TestParts Sales Company; http://www.testparts.com/ ; 126 Railroad St., P.O. Box 425, Thomson, GA 30824 USA
TN	Telnochek, Pavel. V. Kolinko, 12610 Torrey Bluff Dr. #380, San Diego, CA, 92130, USA; e-mail: pkolinko@hotmail.com

- [1] M. Oxborrow, “Whispering gallery oscillator (using paramagnetic ions),” *UK Patent GB 2425221 A and US Patent 7292112*, 2005-2009.
- [2] P.-Y. Bourgeois, M. Oxborrow, N. Bazin, Y. Kersalé, and V. Giordano, “Observation of a bistability effect in a cryogenic whispering gallery mode resonator,” in *Proc. of 19th European Frequency and Time Forum*, Besançon, France, 2005, pp. 141-144.
- [3] G. J. Dick and R. T. Wang, “Ultra-Stable Performance of the Superconducting Cavity Maser,” *IEEE Trans. Instrum. Meas.*, vol. 40, pp. 174-177, April 1991.
- [4] D. L. Creedon, K. Benmessaï, M. E. Tobar *et al*, “High power solid-state sapphire Whispering Gallery mode maser” in *Proceedings of Joint F C S (2009) and 22nd EFTF*, Besançon, France, 2009, pp. 282 - 285
- [5] A. E. Siegman, *Microwave Solid-state Masers*, McGraw-Hill, 1964.
- [6] F. Schmid and D. J. Viechnicki, “A New Approach to High Temperature Crystal Growth from the Melt,” *Solid State Technology*, vol. 16, pp. 45-48, September 1973.
- [7] J. L. Emmett and T. R. Douthit, “Heat Treating the Sapphire of Rock Creek, Montana,” in *Gems & Gemology*. vol. Winter 1993, 1993, pp. 250-271.
- [8] J. L. Emmett, K. Scarratt, S. F. McClure, *et al* “Beryllium diffusion of ruby and sapphire,” *Gems & Gemology*, vol. Summer 2003, pp. 84-135.
- [9] Lenton, PO Box 2031, Hope Valley, S33 6BW, United Kingdom, www.lenton.com.
- [10] M. W. Dixon, *Microwave Handbook, Vols. 1-3*: Radio Society of Great Britain, 1992.
- [11] R. F. Wenzel, “Second Moment of the Cr^{3+} EPR Line in Ruby Broadened by Strong Hyperfine Interactions,” *Phys. Rev. B.*, vol. 1, pp. 3109-3116, 1970.

- [12] J. Hess and A. Levy, "Response of the Mössbauer spectrum of paramagnetic Fe^{3+} in Al_2O_3 to nuclear dipole fields," *Phys. Rev. B*, vol. 22, pp. 5068-5078, 1980.
- [13] W. J. C. Grant and M. W. P. Strandberg, "Line Shapes of Paramagnetic Resonances of Chromium in Ruby," *Physical Review*, vol. 135, pp. A727-A739, 1964.
- [14] J. Lambe, N. Laurance, E. C. McIrvine, and R. W. Terhune, "Mechanisms of Double Resonance in Solids," *Phys. Rev.*, vol. 122, pp. 1161-1170, 1961.
- [15] C. M. Verber, H. P. Mahon, and W. H. Tantilla, "Nuclear Resonance of Aluminium in Synthetic Ruby," *Phys. Rev.*, vol. 125, pp. 1149-1157, 1962.
- [16] P. L. Donoho, "Spin-lattice Relaxation in Ruby," *Phys. Rev.*, vol. 133, p. A1080, 1964.
- [17] R. Boscaino and F. M. Gelardi, "The spin packet lineshape in dilute ruby samples," *J. Phys. C: Solid State Phys.*, vol. 15, pp. 6245-6255, 1982.
- [18] L. Allen and J. H. Eberly, *Optical resonance and two-level atoms*: John Wiley and Sons, Inc., 1975.
- [19] P. F. Liao and S. R. Hartmann, "Magnetic field- and concentration-dependent photon echo relaxation in ruby with simple exponential decay," *Optics Comm.*, vol. 8, pp. 310-311, 1973.
- [20] S. Clough and C. A. Scott, "Saturation and spectral diffusion in electron spin resonance," *J. Phys. C (Proc. Phys. Soc.)*, Ser. 2, vol. 1, pp. 919-931, 1968.
- [21] R. Boscaino and F. M. Gelardi, "Free-induction decay after saturation in dilute ruby," *Phys. Rev. A*, vol. 45, pp. 546-549, 1992.
- [22] A. Szabo and R. Kaarli, "Optical hole burning and spectral diffusion in ruby," *Phys. Rev. B*, vol. 44, pp. 12307-12313, 1991.
- [23] A. Szabo, T. Muramoto, and R. Kaarli, " ^{27}Al nuclear-spin dephasing in the ruby frozen core and Cr^{3+} spin-flip-time measurements," *Phys. Rev. B*, vol. 42, pp. 7769-7776, 1990.
- [24] H. F. Symmons and G. S. Bogle, "On the Exactness of the Spin-Hamiltonian Description of Fe^{3+} in Sapphire," *Proc. Phys. Soc.*, vol. 79, pp. 468-472, 1962.
- [25] L. S. Kornienko and A. M. Prokhorov, "Electronic Paramagnetic Resonance of the Fe^{3+} Ion in Corundum," *Sov. Phys. JETP*, vol. 13, pp. 1120-1125, 1961.
- [26] G. S. Bogle and H. F. Symmons, "Paramagnetic Resonance of Fe^{3+} in Sapphire at Low Temperatures," *Proc. Phys. Soc.*, vol. 73, pp. 531-532, 1959.
- [27] K. J. Standley and R. A. Vaughan, "Effect of Crystal-Growth Method on Electron Spin Relaxation in Ruby," *Physical Review*, vol. 139, pp. A 1275-1280, 1965.
- [28] P. F. Liao and S. R. Hartmann, "Determination of the Cr-Al Hyperfine Electric Quadruple Interaction Parameters in Ruby Using Spin-Echo Electron-Nuclear Double Resonance," *Phys. Rev. B* vol. 8, pp. 69-80, 1973.
- [29] P. F. Liao, P. Hu, R. Leigh, and S. R. Hartmann, "Photon echo nuclear double resonance and its applications in ruby," *Phys. Rev. A*, vol. 9, pp. 332-340, 1974.
- [30] M. Oxborrow, *unpublished work*, 2009.
- [31] T. Endo, T. Hashi, and T. Muramoto, "Measurement of electron spin-spin relaxation by an optical labeling technique," *Phys. Rev. B* vol. 30, pp. 2983-2985, 1984.
- [32] R. Boscaino and F. M. Gelardi, "Structure and Dynamics of Molecular Systems," 1985.
- [33] K. Benmessaï, D. L. Creedon, M. E. Tobar, P.-Y. Bourgeois, Y. Kersalé, and V. Giordano, "Measurement of the Fundamental Thermal Noise Limit in a Cryogenic Sapphire Frequency Standard Using Bimodal Maser Oscillations," *Phys. Rev. Lett.*, vol. 100, p. 233901, 2008.
- [34] D. J. Howarth and R. Hensman, "Properties of Ferric Ions in Alumina I: Energy Levels and Transition Rates," Royal Radar Establishment, Malvern, Worcs., UK; archived at DSTL Porton Down Information Centre, Porton Down, Salisbury, Wilts., UK April 1960.
- [35] F. Benabid, M. Notcutt, V. Lorient, *et al*, "X-ray induced absorption of high-purity sapphire and investigation of the origin of the residual absorption at 1064 nm," *J. Phys. D: Appl. Phys.*, vol. 33, pp. 589-594, 2000.
- [36] L. V. Nikolskaya, V. M. Terekhova, and M. I. Samoilovich, "On the Origin of Natural Sapphire Color," *Phys. Chem. Minerals*, vol. 3, pp. 213-224, 1978.
- [37] J. J. Krebs and W. G. Maisch, "Exchange Effects in the Optical-Absorption Spectrum of Fe^{3+} in Al_2O_3 ," *Phys. Rev. B.*, vol. 4, pp. 757-769, 1971.
- [38] G. Lehman and H. Harder, "Optical spectra of di and trivalent iron in corundum," *Am. Mineral.*, vol. 55, pp. 98-105, 1970.
- [39] H. H. Tippins, "Charge-Transfer Spectra of Transition-Metal Ions in Corundum," *Phys. Rev. B*, vol. 1, pp. 126-135, 1970.
- [40] R. F. Blunt, G. A. Candela, R. A. Forman, *et al* "Magnetic Susceptibility and Optical Studies of Cr^{3+} in Al_2O_3 (Ruby): Magnetic Method for Determining Concentration," *J. Appl. Phys.*, vol. 42, pp. 3058-3062, 1971.